Computers and Geotechnics 173 (2024) 106515

Contents lists available at ScienceDirect

Computers and Geotechnics

journal homepage: www.elsevier.com/locate/compgeo

Research Paper

Effect of soil stiffness on end bearing resistance of foundations in clay from large deformation numerical modelling

Shujin Zhou, Wangcheng Zhang *, Ashraf S. Osman

Department of Engineering, Durham University, South Road, Durham DH1 3LE, UK

ARTICLE INFO

Keywords:
Clay
Soil stiffness
End bearing resistance
Numerical modelling
Large deformation finite element method

ABSTRACT

Accurately predicting the installation resistance is of great benefit to a rational and economical design of foundations. This research performs a large-deformation finite-element analysis to investigate the effect of soil stiffness on the end bearing resistance in uniform clay. Different types of geotechnical structures and foundations, e.g., cone penetrometer, strip foundation, bucket foundation, and deep piled foundation are considered. Results show that soil stiffness has a negligible impact during shallow penetration but becomes pronounced at deep penetration. It is found that for strip footings, effect of soil stiffness is minimal, whereas the end bearing resistances of CPT and deep piled foundation with a partial plug are highly dependent on the soil stiffness. For a rough pile foundation, the resistance factor $N_{c,pf}$ increases by approximately 30% as soil rigidity I_r increases from 50 to 500. For a bucket foundation, the effect of soil stiffness on the end bearing resistance falls between that of "shallow" and "deep" foundations. Based on the numerical results, empirical expressions are proposed to predict the end bearing resistance factor accounting for the effect of soil stiffness.

1. Introduction

Accurately predicting the bearing capacity of a foundation is important for its design and application (Li et al., 2023; Wang et al., 2023; Yang et al., 2024). The bearing capacity problem was firstly studied for a strip foundation based on the plasticity approach proposed by Prandtl (1920) and further developed and employed for various foundation types (e.g., circular foundation, square foundation, and rectangular foundation) with empirical factors (e.g., shape factor and depth factor) (Meyerhof, 1951; Skempton, 1951; Salgado et al., 2004; Edwards et al., 2005). For clays, the bearing capacity can be described as:

$$q_{net} = q_u - q_0 = s_c d_c N_{c0} s_u = N_c s_u \tag{1}$$

where q_{net} is the net ultimate unit base resistance; q_u is the total ultimate unit base resistance; q_0 is the surcharge at the foundation base level; s_c is a shape factor, taken as unity for strip footing; d_c is a depth factor, equal to unity for a surface footing; s_u is the undrained shear strength of clay at the foundation base; N_{c0} is the bearing capacity factor for a surface strip footing, taken as $\pi+2$ according to an exact solution found by Prandtl (1920); and N_c is the net bearing capacity factor.

The soil stiffness, related to initial mean effective stress p', undrained shear strength s_u, and over-consolidation ratio OCR, plays an important role in many geotechnical engineering problems (Vardanega and Bolton, 2013; Cheng et al., 2023). Viggiani and Atkinson (1995) proposed an empirical correlation for maximum shear modulus G_{max} with OCR and mean effective stress, written as

$$\frac{G_{max}}{p'_r} = A\left(\frac{p'}{p'_r}\right)^n \mathrm{OCR}^m \tag{2}$$

where p'_r is the reference pressure, taken as 1 kPa; n and m are the constants that depend on clay type such as plasticity index; A is a factor accounting for clay structure. Besides, the effect of stiffness is crucial in the foundation settlement analysis (Paice et al., 1996), spudcan-pile interaction analysis (Tho et al., 2013), and in the cavity expansion analysis of pressuremeter test, pile installation or cone penetration test (Houlsby and Wroth, 1991).

Solutions from plastic limit theorems have implied that the rigidity of the clay soil has no impact on the ultimate bearing capacity factors, which have been confirmed through small strain finite element (SSFE) analyses (Bransby and Randolph, 1999; Zhang et al., 2012; Liu et al., 2017). A few studies found that soil stiffness affects the initial load–displacement response but has little or no effect on the ultimate bearing capacity (Edwards et al., 2005; Salehi et al., 2018). This seems

* Corresponding author.
E-mail addresses: shujin.zhou@durham.ac.uk (S. Zhou), wangcheng.zhang@durham.ac.uk (W. Zhang), ashraf.osman@durham.ac.uk (A.S. Osman).

https://doi.org/10.1016/j.compgeo.2024.106515
Received 10 January 2024; Received in revised form 3 June 2024; Accepted 5 June 2024
Available online 14 June 2024

reasonable for a shallow foundation, as it takes a small displacement to reach the load limit. However, for a deeply buried foundation, the ultimate bearing capacity is reached at a large displacement, whereby SSFE analysis may not be adequate. For example, Edwards et al. (2005) implied that, in undrained clay with soil rigidity $I_r = 167$, a circular foundation with a pre-embedded depth of 4D reaches the ultimate bearing capacity at a displacement of approximately 2.5D. An artificially increased soil stiffness is usually used in the SSFE analysis to ensure that the plastic failure occurs at a small displacement (e.g., Zhang et al., 2012; Li et al., 2021), assuming the stiffness has no effect on the bearing capacity.

Some studies have found that the bearing capacity of foundations, e.g., strip footing (Wang and Carter, 2002) and bucket foundation (Xiao et al., 2019), varies considerably with the soil stiffness through large deformation finite element (LDFE) analyses in contrast to the SSFE analyses. A study by Ullah et al. (2020) examined the effect of stiffness on the bearing capacity of a rectangular foundation and revealed that the clay stiffness has no influence on bearing capacity at shallow bury depth. For a deep foundation, they addressed higher stiffness results in a lower bearing capacity factor.

The fact that soil stiffness has minimal impact on the bearing capacity of a foundation at a shallow depth but becomes significant when it is deeply buried is attributed to the nature of the evolving soil flow mechanisms. For a shallow foundation, where an SSFE analysis is adequate, the failure plane is distinctly established and the load–displacement curve shows a plateau at yielding. In contrast, for a deep foundation, where an LDFE analysis is needed, the full failure mechanism involving soil flow can be observed only through continuous penetration with an evolving plastic zone and a hardening load–displacement relationship. It is recognized that for a circular foundation with embedded depth larger than 2D it is not possible to reach the limit load in SSFE analysis, even after a displacement of 0.3D, as the bearing capacity factors can only be mobilized at a certain foundation displacement (Hu et al., 1999; Edwards et al., 2005). In an SSFE analysis, such a significant displacement can lead to mesh distortion and hence unreliable numerical results. A large deformation analysis is therefore necessary to investigate the ultimate bearing capacity of a deep foundation.

This paper presents a comprehensive study on the effect of soil stiffness on the ultimate end bearing capacity of foundations penetrating in uniform clays. Various types of geotechnical structures or foundations, e.g., cone penetrometer, strip foundation, bucket foundation, and pile foundation, are considered and their penetration processes are investigated through LDFE analyses. The numerical analyses yield empirical expressions designed to enhance the estimation of bearing capacity factors for various geotechnical foundations, taking into account the effects of soil stiffness.

2. Numerical modelling

2.1. LDFE analyses

Geotechnical applications often involve significant displacement of structural elements. Quantification of soil-structure interaction must, therefore, consider geometric nonlinearity arising from alterations in the surface profile or material distribution. To tackle the difficulty of excessive mesh distortion in traditional SSFE method, substantial efforts have been made on the LDFE analysis, such as the Arbitrary Lagrangian Eulerian (ALE) method (Fan et al., 2021), the material point method (MPM) (Phuong et al., 2014), the coupled Eulerian-Lagrangian (CEL) method (Zhou et al., 2021), and Smoothed Particle Hydrodynamics (SPH) (Zhang and Randolph, 2020). In this study, the RITSS method (remeshing and interpolation technique with small strain (Hu and Randolph, 1998)) is developed and implemented in the commercial software ABAQUS, where the whole analysis is divided into a series of incremental small strain analysis combined with frequent remeshing of the entire domain, followed by the update of all field variables (i.e., stresses and material properties) from the old mesh to the new mesh. The accuracy of LDFE analysis with RITSS depends on the interpolation technique employed to update field variables from the old to new mesh. In this study, the field variables such as stresses and material properties are interpolated linearly from the old integration points to the new integration points through a Gauss mesh formed by Delaunay triangulation (Lee and Schachter, 1980; Sloan, 1993) of all the old integration points. For those new integration points close to the edge but falling outside the Gauss mesh, we simply recover the field variables from the nearest old integration points. This method is similar to the non-unique element method (Zhou, 2008), and the robustness of this technique has been validated by Zhou (2008) and Zhang et al. (2015). The advantage of RITSS lies in its versatility, as the remeshing and interpolation processes can be undertaken by any programming language and implemented into commonly used FE platforms, such as AFENA, ABAQUS and ANSYS (Hu and Randolph, 1998; Yu et al., 2008; Wang et al., 2010). The comparison of RITSS with other LDFE methods has been reviewed by Wang et al. (2015) through some benchmark cases.

2.2. Geometry and parameters

Numerical models of the cone penetrometer, strip footing, bucket foundation, and pile foundation are detailed in this section and shown in Fig. 1. The piezocone model has a cone area of 1500 mm^2 (diameter D = 43·7 mm, typical for offshore practice) and a tip–apex angle of 60°. The strip footing has a width of $B = 1$ m, and the target penetration depth is 5B. Two pile models are considered: the bucket foundation has a diameter of $D = 10$ m, a length of $L = 10$ m (i.e., $L/D = 1.0$), and a wall thickness of $t = 0.2$ m (i.e., $D/t = 50$); while a relatively small-diameter pile foundation has a diameter of $D = 1$ m, a length of $L = 10$ m (i.e., $L/D = 10$), and a wall thickness of $t = 0.02$ m (i.e., $D/t = 50$). The foundation structures are simplified as rigid bodies since their stiffness greatly exceeds that of the soil.

For CPT and pile foundation cases, an axisymmetric soil domain of 15 m in radius and 30 m in depth is chosen; while for the bucket foundation case, a domain of 60 m × 60 m is used to ensure that the domain boundaries are well outside the soil plastic zone. Half of the soil domain with 15 m in width and 30 m in depth is taken for the strip foundation modelling and it is treated as a plane strain problem. Hinge and roller conditions are applied along the base and two sides of the soil domain, respectively. Linear four-node quadrilateral elements (CAX4 for axisymmetric problems and CPE4 for plane strain problems) with four internal Gauss points are used in the FE analyses. A fine mesh is defined around the cone/pile tip to ensure the accuracy of the numerical results, and the sub-refinement zone is set along the shaft. Fig. 1 displays the representative mesh and boundary conditions for cases of CPT, strip footing, bucket foundation, and pile foundation, respectively. It is noted that the structures are slightly buried in soil to facilitate numerical modelling (i.e., 0.1B (or 0.1D) for strip footing and bucket foundation, 1D for CPT and pile foundation). The sharp tips/edges of structures have been slightly smoothed, as shown in Fig. 1, to improve numerical convergence.

The soil is modelled as a linear elastic-perfectly plastic material obeying a Tresca yield criterion. Considering the relatively fast penetration rate, undrained soil condition is considered with a Poisson's ratio of $\nu = 0.495$. The undrained soil strength is taken as $s_u = 5$ kPa with a submerged soil density $\rho' = 600$ kg/m^3. For simplification, only smooth (i.e., frictionless or $\alpha = 0$, where α is the adhesion factor) and rough (i.e., fully bonded or $\alpha = 1$) soil-structure interfaces are simulated. In each incremental Lagrangian calculation, there are two analysis steps, including the geostatic step and the penetrating step. The initial geostatic stress condition is achieved by assuming the coefficient of earth pressure at rest $K_0 = 1$. Displacement is applied at a specified load reference point (LRP) in each case to control the foundation movements and the reaction force can be obtained at the LRP.

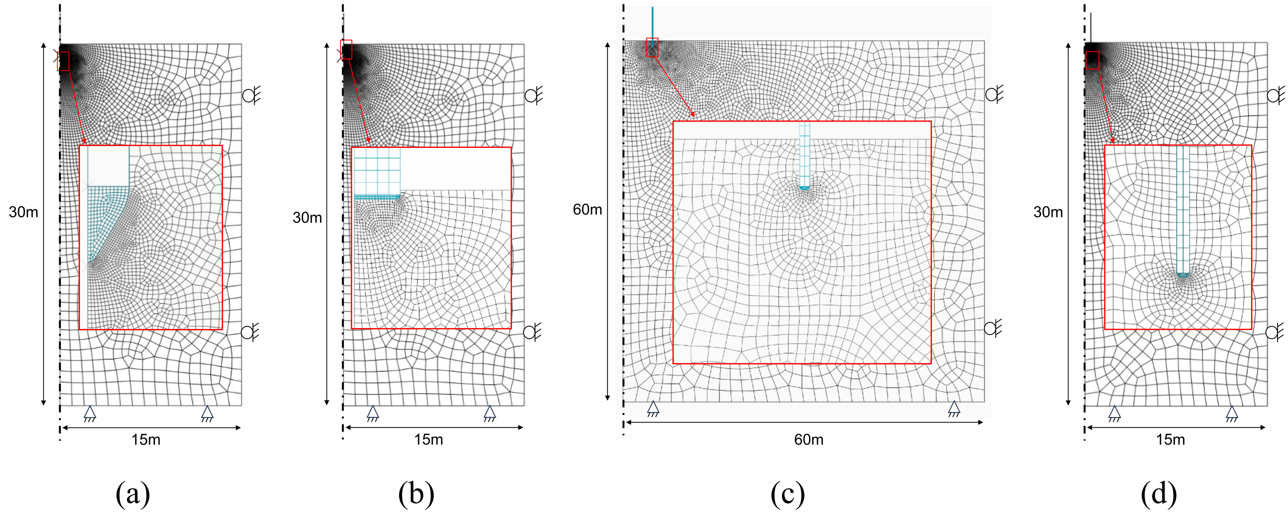

Fig. 1. Numerical model used in the LDFE analysis: (a) CPT; (b) strip foundation; (c) bucket foundation; (d) pile foundation.

Based on experimental data (Duncan and Buchignani, 1976; Ladd et al., 1977; Casey et al., 2016) depicted in Fig. 2, a typical range of the rigidity index I_r is from 50 to 500, which is also in consistent with some previous studies (Lu et al., 2004; Ma et al., 2016). Parametric studies, in terms of the rigidity index I_r (varying between 50, 100, 167, 200, 300, and 500), are carried out to investigate its effect on the end bearing resistances of various geotechnical structures at different depths.

3. Results and discussion

3.1. Cone penetration test

CPT is commonly employed to measure in situ soil properties such as strength, with the advantage of avoiding uncertainties in contrast to the lab elementary tests based on disturbed soil samples. It supplies a nearly continuous record of the resistance with depth and has a strong theoretical background. In practice, the deep penetration resistance factor is of interest for engineering design, and in the study a penetration depth ratio of $d/D = 20$ is focused. Cavity expansion theory has been proved to be suitable for estimating the cone factor at deep penetration, which has acknowledged that the soil stiffness has an effect on the end bearing resistance because the magnitude of cavity expansion strain is highly dependent on the radius of failing soils (Teh and Houlsby, 1991).

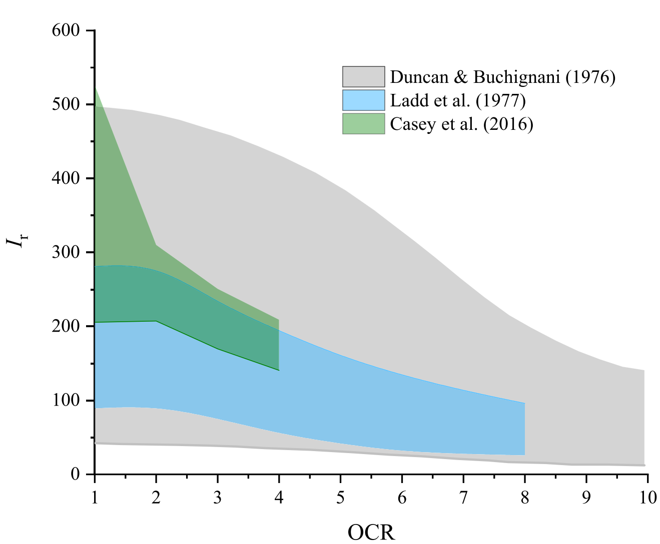

Fig. 2. Rigidity index variation for undrained clays (after Casey et al. (2016)).

Fig. 3 shows the failure mechanisms at a penetration depth of $d/D = 20$ for $I_r = 50$ and 500. The contour of maximum shear stress ($(\sigma_1 - \sigma_3)/2$, where σ_1 and σ_3 denote the maximum and minimum principal stresses, respectively) indicates that the plastic zone is localized around the cone tip, and the range of mobilized soil of the case with $I_r = 500$ is evidently larger than that of $I_r = 50$. According to Lunne et al. (2002), the sphere of influence can be as small as two or three times of cone diameters in soft soils, while it may expand to 10 to 20 times cone diameters in stiff soils.

Numerical analyses of CPT from the ground surface to a certain depth ($d/D = 40$) with various rigidity index I_r of 50, 100, 200, 300 and 500 are conducted to explore the effect of soil stiffness. Fig. 4a and b show the penetration resistance factor, $N_{c,CPT}$, over normalized cone penetration depth, d/D, for smooth and rough cones, respectively. It can be seen that the influences of soil stiffness on a smooth cone and a rough cone are comparable. The value of $N_{c,CPT}$ gradually increases with the penetration depth and achieves a steady-state condition at a depth of $d/D = 5$ for $I_r = 50$, where a transition mechanism from shallow penetration to deep penetration occurs; while $N_{c,CPT}$ continues to rise until $d/D = 15$ for $I_r =$

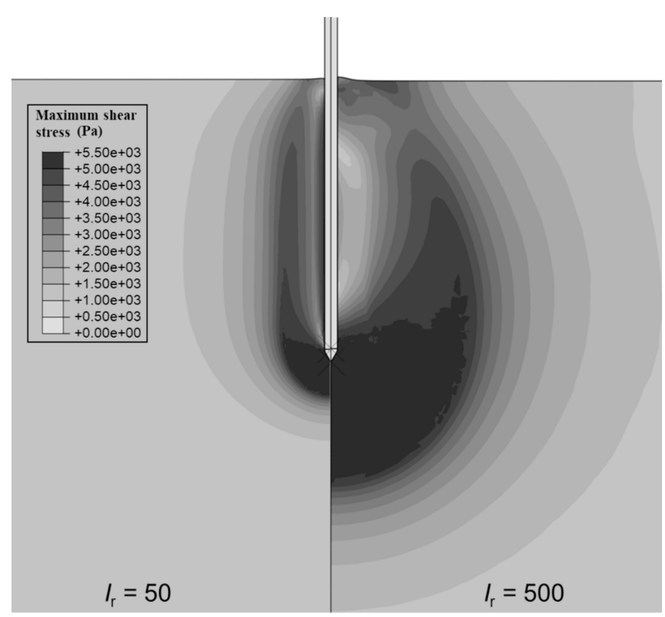

Fig. 3. Maximum shear stress contours of CPT penetration at a depth of $d/D = 20$.

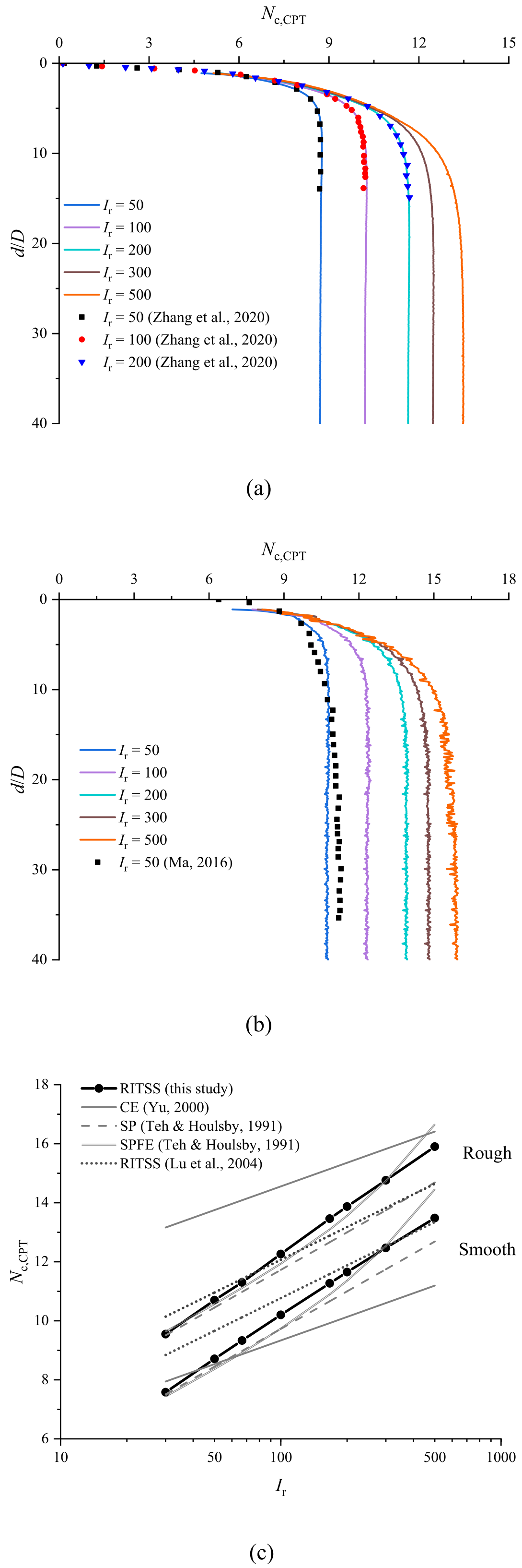

Fig. 4. Effect of soil stiffness on bearing factor of CPT: (a) $N_{c,CPT}$ at various depths for a smooth cone; (b) $N_{c,CPT}$ at various depths for a rough cone; (c) deep bearing factor $N_{c,CPT}$ plotted against rigidity index I_r compared to previous studies (CE: cavity expansion theory; SP: strain path method; SPFE: strain path finite element method).

500. This indicates that the critical depth for a deep failure mechanism increases as soil stiffness rises. Numerical results from previous studies (Ma, 2016; Zhang et al., 2022) have also been included for comparison, where close agreement can be obtained. The deep penetration resistance factor is shown and compared with existing theoretical solutions including the cavity expansion method, strain path method and strain path finite element method in Fig. 4c. It can be seen that, the end bearing resistance factors derived from the present work generally agree well with the solution from the strain path method by Teh and Houlsby (1991), the hybrid strain path and FE analysis by Teh and Houlsby (1991), and RITSS method by Lu et al. (2004). The values of $N_{c,\,CPT}$ also fall within the range of the results from the cavity expansion method by Yu (2000). A slight difference between this study and that of Lu et al. (2004) is found, possibly due to different mesh strategy, interpolation methods, contact algorithms, etc. The fitting curve for the cone factor is given by

$$N_{c,\,CPT} = \begin{cases} 1.96\ln(I_r) + 1.13(\text{smooth}) \\ 1.96\ln(I_r) + 3.33(\text{rough}) \end{cases} \tag{3}$$

The above fitting results indicate that the gradient of $N_{c,\,CPT}$ against $\ln I_r$ is almost independent of cone roughness while the intercept increases with the roughness.

3.2. Strip footing

Previous studies have indicated that the bearing capacity factor of a shallow foundation is independent of soil stiffness (Bransby and Randolph, 1999; Edwards et al., 2005; Ullah et al., 2020) since shallow penetration involves a mechanism where slip surfaces predominantly extend outwards and upwards to the ground surface. When the foundation is placed at a considerable depth, however, a deep failure mechanism occurs, and the plastic zone is localized around the tip of the foundation. The effect of the soil deformation (leading to local shear failure as a deep failure mechanism) on the bearing capacity factor of a deep strip foundation can be obtained by the cavity expansion theory proposed by Bishop et al. (1945). The expression for $N_{c,sf}$ is given by

$$N_{c,\,sf} = \ln(I_r) + 2 \tag{4}$$

For typical clays with I_r varying from 50 to 300, Eq. (4) gives a range for $N_{c,sf}$ from 5.91 to 7.70. This range is somewhat lower than the range from 8.28 to 8.85 for a deep strip foundation proposed by Meyerhof (1951) using bearing capacity theory.

The maximum shear stress contours of a strip foundation with rough contact at a depth of $d/B = 5$ for $I_r = 50$ and 500 are shown in Fig. 5. It is shown that the yielding zone of $I_r = 500$ is larger than that of $I_r = 50$, as is the extent of soil heaving. Fig. 6a and b show the end bearing resistance factor, $N_{c,sf}$, over normalized penetration depth, d/B, for smooth and rough foundation-soil interfaces, respectively. It is evident that as the penetration depth increases, the end bearing factor rises at a diminishing rate. The end bearing factor increases slightly with soil stiffness, but when I_r surpasses 100, this influence becomes negligible. This may explain the historical lack of research examining the effect of soil stiffness on the end bearing resistance in clay. The impact of soil stiffness is more pronounced for a rough strip foundation compared to a smooth strip foundation. The findings from existing publications, including the mechanism-based method (Meyerhof, 1951) and finite element limit analysis (Salgado et al., 2004) without considering the stiffness effect are incorporated for comparison, where close agreement is achieved.

Results from the current study indicate a correlation between $N_{c,sf}$ (at depths of $d/B = 0.5$ and 5) and I_r for a strip footing given by the following equations.

For a strip footing at a depth of $d/B = 0.5$:

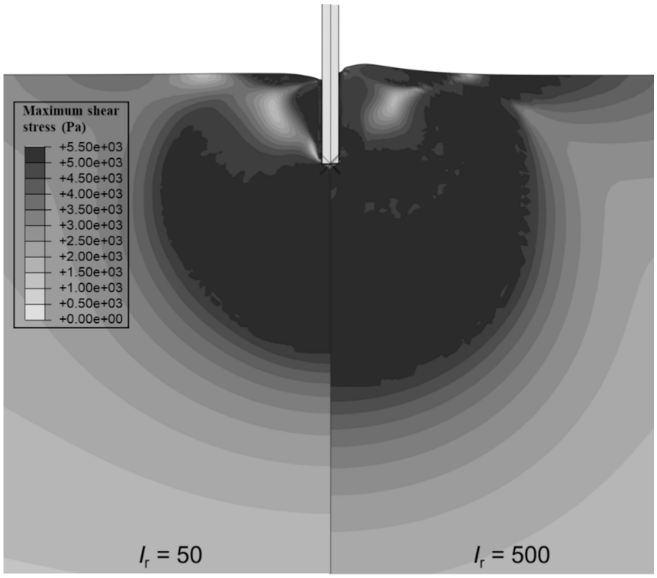

Fig. 5. Maximum shear stress contours of a strip foundation at a depth of $d/B = 5$.

$$N_{c,sf} = \begin{cases} 0.22\ln(I_r) + 4.95(\text{smooth}) \\ 0.22\ln(I_r) + 5.14(\text{rough}) \end{cases} \tag{5}$$

For a strip footing at a depth of $d/B = 5$:

$$N_{c,sf} = \begin{cases} 0.31\ln(I_r) + 6.62(\text{smooth}) \\ 0.31\ln(I_r) + 7.37(\text{rough}) \end{cases} \tag{6}$$

Fig. 6c compares the predicted $N_{c,sf}$ values using Eqs. (5) and (6) with the LDFE analyses results, where reasonably good agreement can be obtained. It is noted that the final penetration depth of a strip foundation in this study is $d/B = 5$, which is deep enough for most strip foundations. It is possible that the stiffness effect may become more significant with increasing depth beyond $d/B = 5$.

3.3. Bucket foundation

Large-diameter piles (bucket foundations) with an aspect ratio L/D less than one are popularly employed in offshore practice as an alternative to deep piled foundations (Randolph and Gourvenec, 2017). This study considers a bucket foundation with $L/D = 1$ penetrating in uniform clay with various stiffness I_r. Fig. 7 shows the maximum shear stress contours of a rough bucket foundation at a penetration depth of $d/D = 1$ for $I_r = 50$ and 500, where both soil heave and plastic area for $I_r = 500$ are larger than that for $I_r = 50$. The responses of $N_{c,bf}$ obtained from a series of cases varying I_r as 50, 100, 167, 200, 300, and 500 are presented in Fig. 8, with Fig. 8a for a smooth bucket foundation and Fig. 8b for a rough bucket foundation. It is noted that increasing the soil stiffness leads to more pronounced fluctuations in the end bearing resistance which is consistent with the numerical results by Ullah et al. (2020). For a smooth bucket foundation, the limiting deep bearing capacity factor is mobilized at a depth of $\sim 0.4D$, while the bearing capacity factor for a rough bucket foundation remains increasing with the depth. This is because the occurrence of a deep failure mechanism for a smooth bucket foundation is related to the wall thickness d/t and almost unaffected by the inner soil, whereas for a rough bucket foundation where a soil plug exists, the bearing capacity factor evolves with depth until soil plug is fully developed acting like a solid pile. The bearing capacity factors for a bucket foundation at depths of $0.5D$ and $1.0D$ are obtained and shown in Fig. 8c, and the relationships between $N_{c,bf}$ and I_r can be best fitted as the following equations.

For a bucket foundation at a depth of $d/D = 0.5$:

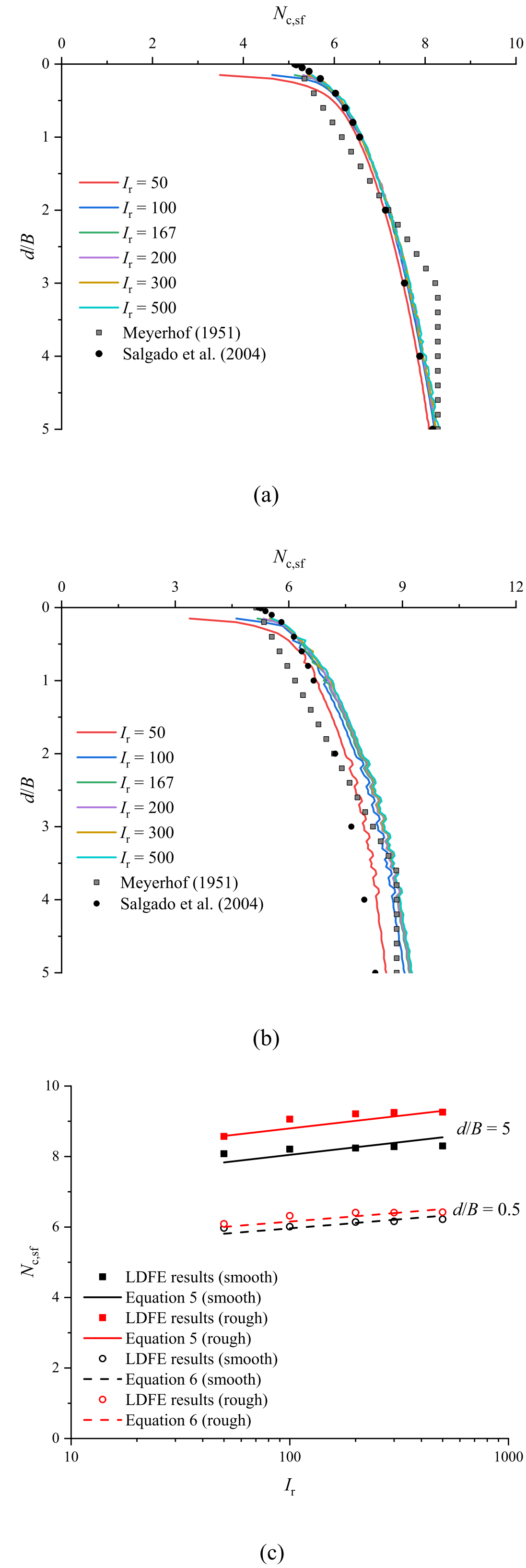

Fig. 6. Effect of soil stiffness on bearing factor of a strip foundation: (a) $N_{c,sf}$ at various depths for a smooth strip foundation; (b) $N_{c,sf}$ at various depths for a rough strip foundation; (c) bearing factors $N_{c,sf}$ plotted against rigidity index I_r.

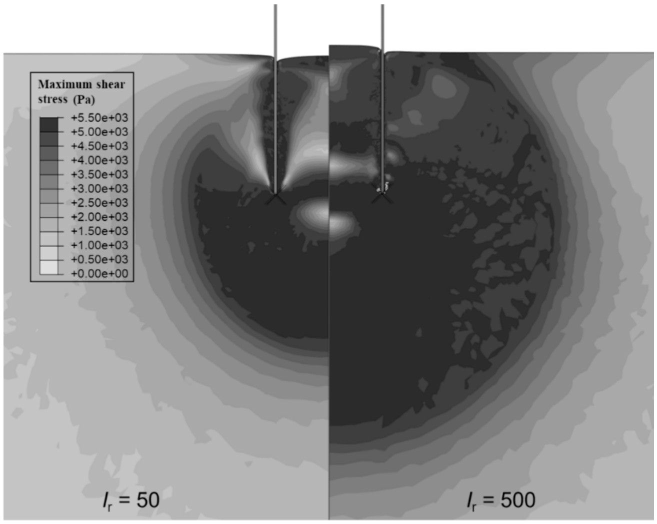

Fig. 7. Maximum shear stress contours of a bucket foundation at a depth of $d/D = 1$.

$$N_{c,bf} = \begin{cases} 0.76\ln(I_r) + 5.33(\text{smooth}) \\ 0.76\ln(I_r) + 7.73(\text{rough}) \end{cases} \tag{7}$$

For a bucket foundation at a depth of $d/D = 1.0$:

$$N_{c,bf} = \begin{cases} 0.99\ln(I_r) + 4.39(\text{smooth}) \\ 0.99\ln(I_r) + 7.77(\text{rough}) \end{cases} \tag{8}$$

3.4. Pile foundation

It is widely accepted that cavity expansion theory can be applied to estimate the bearing capacity of solid piles in soils like CPT (Yu, 2000), and it has also been used to predict the radial stress and radial displacements of a thin-walled open-ended pile (Chen and Randolph, 2007; Randolph, 2003).

In this section, the influence of soil stiffness on end bearing resistance of a pipe pile is investigated by varying I_r. The pile foundation has an aspect ratio of $L/D = 10$, which is pre-embedded in the soil at a depth of $1D$ to reduce computation time. The maximum shear stress contours for $I_r = 50$ and 500 are depicted in Fig. 9, with Fig. 9a representing the case of a smooth pile and Fig. 9b corresponding to a rough pile. A significant soil heave is observed for a smooth pile in Fig. 9a, and the height of soil heave for $I_r = 500$ is larger than that for $I_r = 50$, while the plastic zone is comparable between $I_r = 50$ and 500. For a rough pile, as shown in Fig. 9b, soil plug occurs inside the pile due to the squeezing of soil at the pile tip. The degree of soil plugging is more severe for a smaller soil stiffness, whereas the plastic area is notably larger for $I_r = 500$ compared to $I_r = 50$. This is because a pile penetrating in the soil with larger stiffness induces a larger amount of radial displacement and consequently generates a higher pressure in the expansion of a cylindrical cavity with more soil flowing into the pile. Fully plugging is not observed in this study, and the pile penetrates in an unplugged (Fig. 9a) or partially plugged (Fig. 9b) manner.

The values of $N_{c,pf}$ for various I_r are plotted in Fig. 10a and b, from which it is shown that the effect of soil stiffness is more obvious for a rough pile than a smooth pile due to the fact that a larger failure zone is developed for a rough pile penetrating in a partially plugged manner compared with a smooth pile. For a smooth pile, as shown in Fig. 10a, the end bearing factor $N_{c,pf}$ slightly increases with depth, possibly attributable to the inner soil heave. The effect of soil stiffness on the bearing capacity of a smooth pile is similar to that on the bearing capacity of a bucket foundation, as both of them are in an unplugged condition. As such, the resistance factor $N_{c,pf}$ for an unplugged pile can be estimated by Eq. (8). In Fig. 10b, the resistance factor $N_{c,pf}$ for a rough

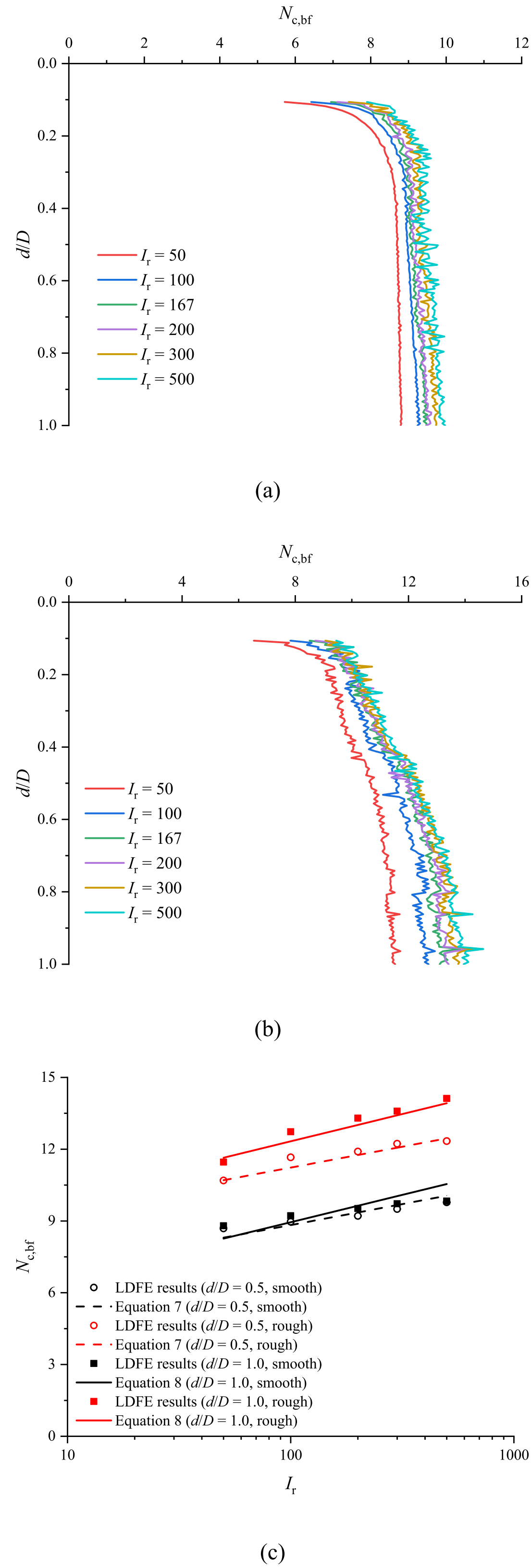

Fig. 8. Effect of soil stiffness on bearing factor of a bucket foundation: (a) $N_{c,bf}$ at various depths for a smooth bucket foundation; (b) $N_{c,bf}$ at various depths for a rough bucket foundation; (c) bearing factor $N_{c,bf}$ plotted against rigidity index I_r.

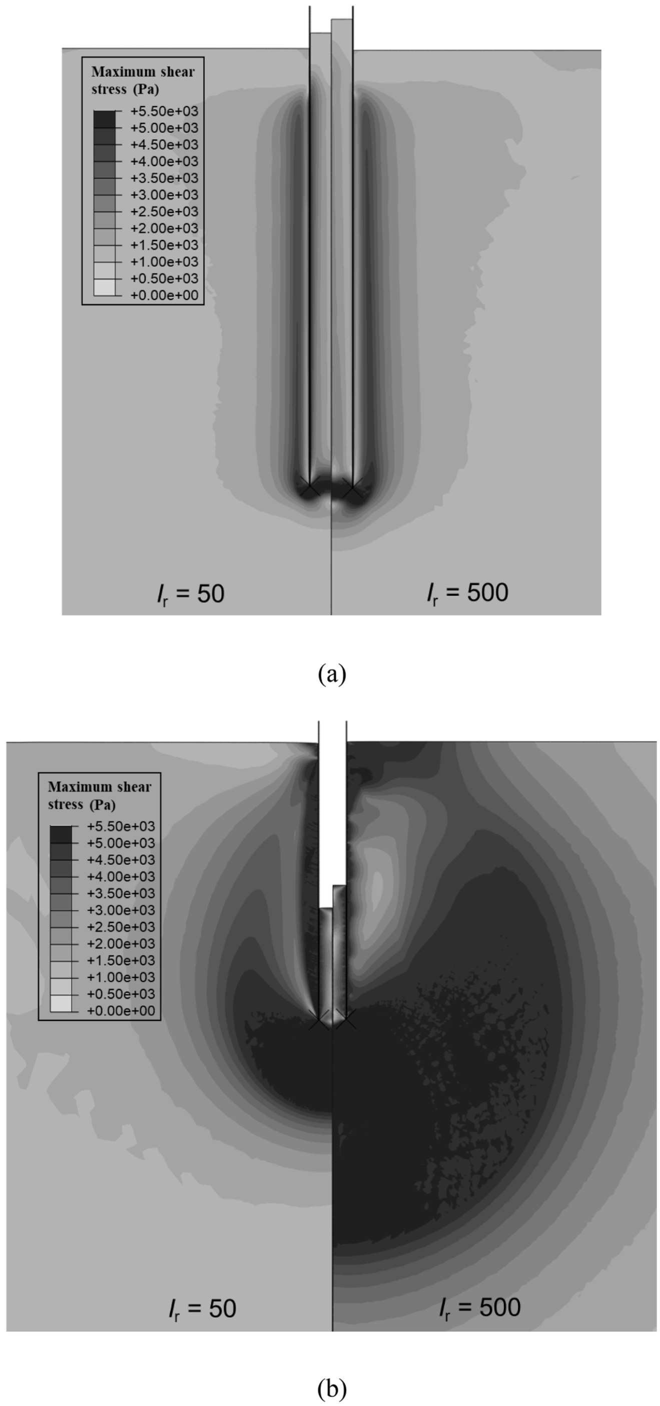

Fig. 9. Maximum shear stress contours of a pile foudantion at a depth of d/D = 10: (a) smooth pile; (b) rough pile.

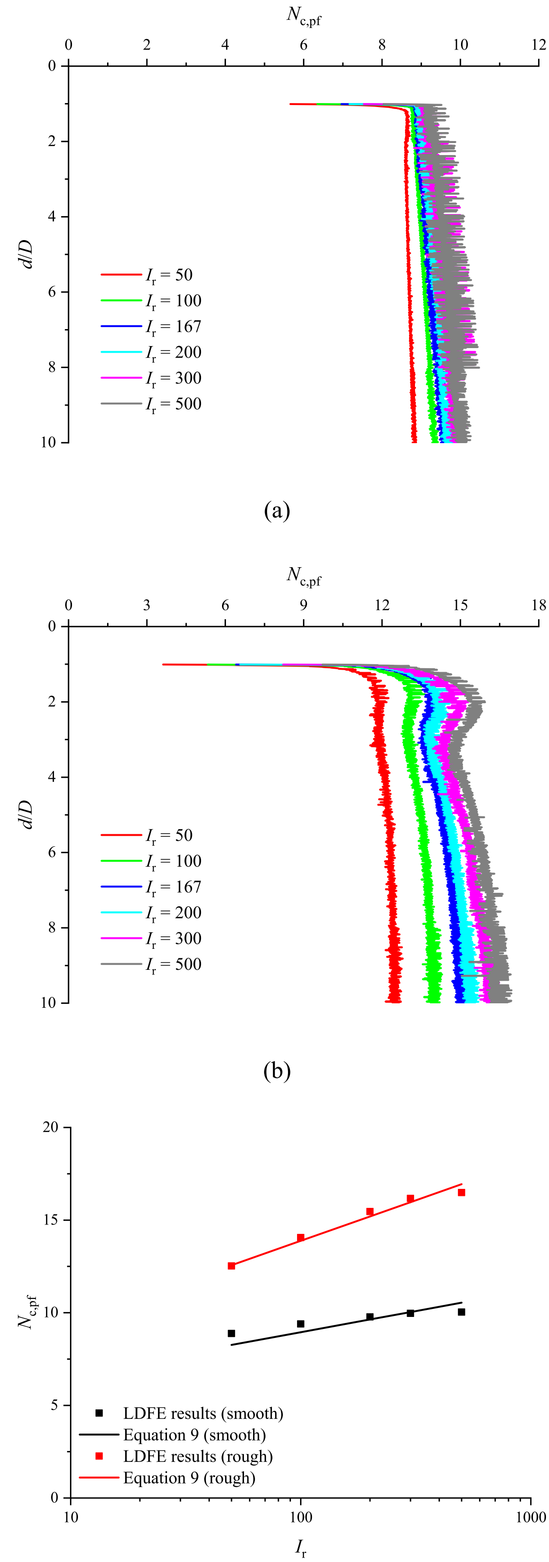

(c)

Fig. 10. Effect of soil stiffness on bearing factor of a pile foundation: (a) $N_{c,pf}$ at various depths for a smooth pile; (b) $N_{c,bf}$ at various depths for a rough pile; (c) deep bearing factor $N_{c,bf}$ plotted against rigidity index I_r.

pile exhibits an initial rise followed by a decline when $d/D < 4$, which might be due to a transition of flow mechanism and the formation of soil plug. It can be inferred that the tip resistance factor $N_{c,pf}$ increases by approximately 12 % for a smooth pile and 30 % for a rough pile, as soil rigidity I_r increases from 50 to 500. Fig. 10c depicts the $N_{c,pf}$ values against the rigidity index (I_r), which can be predicted as

$$N_{c,pf} = \begin{cases} 0.99\ln(I_r) + 4.39(\text{smooth}) \\ 1.90\ln(I_r) + 5.13(\text{rough}) \end{cases} \quad (9)$$

The rigidity index I_r, obtained through e.g. triaxial compression and direct shear tests, can be used to determine the bearing resistance factor through the proposed equations. The empirical expressions cover a practical range of soil stiffness and can be used for engineering design.

4. Discussion

The effect of soil stiffness on the end bearing resistance of various geotechnical structures or foundations at different depths has been thoroughly investigated. For a strip footing, the effect of soil stiffness is not obvious in the practical embedded depths (e.g., 0.5B) as the end bearing factor for a rough strip footing increases from 6.09 to 6.42 with the rigidity index increasing from 50 to 500. For a bucket foundation, as an intermediate offshore foundation (Kay et al., 2021), the effect of soil stiffness falls between that of "shallow" and "deep" foundations, with the end bearing factor increasing by approximately 15 % for a rough bucket foundation with $d/D = 0.5$, as soil rigidity I_r increases from 50 to 500. For CPTs and pile foundations, however, the end bearing resistances are highly dependent on the soil stiffness. Results show that the bearing capacity of a shallow foundation is less affected by the soil stiffness with a shallow failure mechanism; a deeply buried foundation, however, exhibits a deep flow mechanism so that the failure zone is influenced by the soil stiffness. With the rigidity index increasing from 50 to 500, the end bearing resistance is enhanced by up to 5 % for shallow foundations and as high as 50 % for deep foundations with rough interface, as shown in Fig. 11.

The observation of the effect of soil stiffness on the end bearing resistance also has a practical meaning for numerical modelling. Small strain analysis with an artificially increased soil stiffness is proper to determine the ultimate bearing capacity of a shallow foundation to reduce the computational cost because the effect of soil stiffness is less significant; while for a deeply buried foundation, the effect of soil stiffness should be considered and artificially increasing the soil stiffness may cause inaccurate estimate of end bearing resistance. In practical design, it is crucial to account for soil stiffness when estimating the bearing capacity of deep foundations; neglecting this factor could result in an overestimation.

5. Concluding remarks

A series of numerical modelling using the Large Deformation Finite Element (LDFE) method with the RITSS (Remeshing and Interpolation Technique with Small Strain) approach are performed to investigate the effect of soil stiffness on the foundation end bearing resistance. Various geotechnical structures at different depths are considered in this study, including CPT, strip foundation, bucket foundation, and deep piled foundation. It is found that soil stiffness has a negligible impact during shallow penetration but becomes pronounced at deep penetration. For CPTs and solid piles, soil stiffness has a significant effect on the bearing capacity factor, which can be explained by cavity expansion theory. For shallow foundations, such as strip footings, soil stiffness has a minimal influence on the bearing capacity. The effect of soil stiffness on the end bearing resistance of a bucket foundation falls between that of "shallow" and "deep" foundations. For a pipe pile foundation, the significance of soil stiffness becomes evident when a soil plug occurs, with the resistance factor $N_{c,pf}$ increasing by approximately 30 % when soil rigidity I_r increases from 50 to 500. Besides, soil stiffness may also affect the soil flow mechanisms (e.g., soil heaving and soil plugging). Based on the numerical results, empirical expressions are derived to quantify the effect of soil stiffness and predict the penetrating resistance factor. All the analyses are undertaken with a smooth or rough structure-soil interface, and the evolution of bearing factors at shallow depths is not considered in the empirical solutions.

CRediT authorship contribution statement

Shujin Zhou: Writing – original draft, Validation, Methodology, Investigation, Formal analysis, Data curation. **Wangcheng Zhang:** Writing – review & editing, Supervision, Project administration, Methodology, Funding acquisition, Conceptualization. **Ashraf S. Osman:** Writing – review & editing, Supervision, Project administration, Funding acquisition.

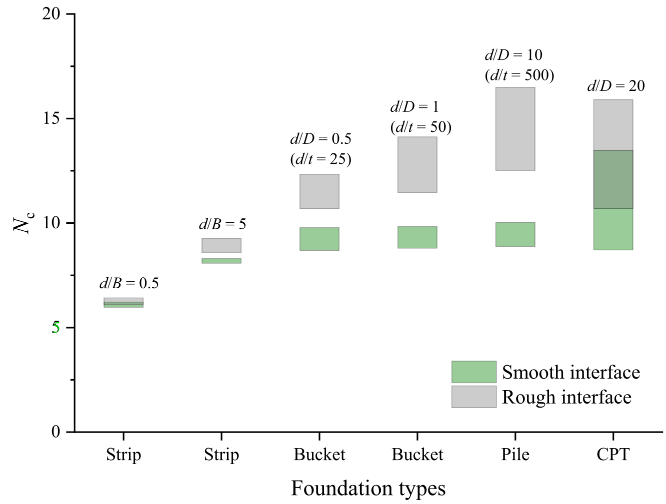

Fig. 11. Effect of soil stiffness on end bearing factors for various foundations (the minimum and maximum values of N_c for each block correspond to $I_r = 50$ and 500, respectively). In the figure, d is the penetration depth, B the width, D the diameter, t the wall thickness of the foundation.

Declaration of competing interest

The authors declare that they have no known competing financial interests or personal relationships that could have appeared to influence the work reported in this paper.

Data availability

Data will be made available on request.

Acknowledgement

The first author is the recipient of the Durham-CSC (China Scholarship Council) Joint PhD Scholarship (CSC 202206150024).

References

Bishop, R.F., Hill, R., Mott, N., 1945. The theory of indentation and hardness tests. Proc. Phys. Soc. 57 (3), 147.

Bransby, F., Randolph, M., 1999. The effect of embedment depth on the undrained response of skirted foundations to combined loading. Soils Found. 39 (4), 19–33.

Casey, B., Germaine, J., Abdulhadi, N., Kontopoulos, N., Jones, C., 2016. Undrained Young's modulus of fine-grained soils. J. Geotech. Geoenviron. Eng. 142 (2), 04015070.

Chen, W., Randolph, M.F., 2007. External radial stress changes and axial capacity for suction caissons in soft clay. Géotechnique 57 (6), 499–511.

Cheng, X., Wang, T., Zhang, J., Wang, P., Tu, W., Li, W., 2023. Dynamic response analysis of monopile offshore wind turbines to seismic and environmental loading considering the stiffness degradation of clay. Comput. Geotech. 155, 105210.

Duncan, J.M., Buchignani, A., 1976. An engineering manual for settlement studies. University of California, Department of Civil Engineering.

Edwards, D., Zdravkovic, L., Potts, D., 2005. Depth factors for undrained bearing capacity. Geotechnique 55 (10), 755–758.

Fan, S., Bienen, B., Randolph, M.F., 2021. Effects of monopile installation on subsequent lateral response in sand. I: Pile installation. J. Geotech. Geoenviron. Eng. 147 (5), 04021021.

Houlsby, G., Wroth, C., 1991. The variation of shear modulus of a clay with pressure and overconsolidation ratio. Soils Found. 31 (3), 138–143.

Hu, Y., Randolph, M., 1998. A practical numerical approach for large deformation problems in soil. Int. J. Numer. Anal. Meth. Geomech. 22 (5), 327–350.

Hu, Y., Randolph, M., Watson, P., 1999. Bearing response of skirted foundation on nonhomogeneous soil. J. Geotech. Geoenviron. Eng. 125 (11), 924–935.

Kay, S., Gourvenec, S., Palix, E., Alderlieste, E., 2021. Intermediate Offshore Foundations. CRC Press.
Ladd, C. C., Foott, R., Ishihara, K., Schlosser, F., and Poulos, H. (1977). Stress-deformation and strength characteristics. Proc., 9th Int. Conf.on Soil Mechanics and Foundation Engineering, Vol. 2, Japanese Society of Soil Mechanics and Foundation Engineering, Tokyo,421–494.
Lee, D.T., Schachter, B.J., 1980. Two algorithms for constructing a Delaunay triangulation. Int. J. Comput. Inform. Sci. 9 (3), 219–242.
Li, L., Liu, H., Jiang, G., Liu, Z., El Naggar, M.H., Wu, W., 2023. Numerical analysis on the mechanical response of grouted connection for pile-bucket foundation. Ocean Eng. 287, 115790.
Li, S., Yu, J., Huang, M., Leung, C.F., 2021. Upper bound analysis of rectangular surface footings on clay with linearly increasing strength. Comput. Geotech. 129, 103896.
Liu, J., Li, M., Hu, Y., Han, C., 2017. Bearing capacity of rectangular footings in uniform clay with deep embedment. Comput. Geotech. 86, 209–218.
Lu, Q., Randolph, M., Hu, Y., Bugarski, I., 2004. A numerical study of cone penetration in clay. Geotechnique 54 (4), 257–267.
Lunne, T., Powell, J.J., Robertson, P.K., 2002. Cone penetration testing in geotechnical practice. CRC Press.
Ma, H., 2016. Large deformation finite element study of cone penetration in multi-layer clays. The University of Western Australia. Ph. D. Thesis,.
Ma, H., Zhou, M., Hu, Y., Shazzad Hossain, M., 2016. Interpretation of layer boundaries and shear strengths for soft-stiff-soft clays using CPT data: LDFE analyses. J. Geotech. Geoenviron. Eng. 142 (1), 04015055.
Meyerhof, G., 1951. The ultimate bearing capacity of foudations. Geotechnique 2 (4), 301–332.
Paice, G.M., Griffiths, D.V., Fenton, G.A., 1996. Finite Element Modeling of Settlements on Spatially Random Soil. J. Geotech. Eng. 122 (9), 777–779.
Phuong, N., Van Tol, A., Elkadi, A., Rohe, A., 2014. Modelling of pile installation using the material point method (MPM). Numer. Methods Geot. Eng. 271, 271–276.
Prandtl, L., 1920. Uber die harte plastischer korper. Nachr. Ges. Wissensch, Gottingen, Math.-phys Klasse 1920, 74–85.
Randolph, M., 2003. Science and empiricism in pile foundation design. Géotechnique 53 (10), 847–875.
Randolph, M., Gourvenec, S., 2017. Offshore geotechnical engineering. CRC Press.
Salehi, A., Hu, Y., Lehane, B., Zania, V., Sovso, S., 2018. The effect of soil stiffness on the undrained bearing capacity of a footing on a layered clay deposit. In: Physical Modelling in Geotechnics, Volume 2.). CRC Press, pp. 1309–1314.
Salgado, R., Lyamin, A., Sloan, S., Yu, H., 2004. Two-and three-dimensional bearing capacity of foundations in clay. Geotechnique 54 (5), 297–306.
Skempton, A. (1951) The bearing capacity of clays. Selected papers on soil mechanics:50-59.
Sloan, S.W., 1993. A fast algorithm for generating constrained Delaunay triangulations. Comput. Struct. 47 (3), 441–450.
Teh, C., Houlsby, G., 1991. An analytical study of the cone penetration test in clay. Geotechnique 41 (1), 17–34.
Tho, K.K., Leung, C.F., Chow, Y.K., Swaddiwudhipong, S., 2013. Eulerian finite element simulation of spudcan–pile interaction. Can. Geotech. J. 50 (6), 595–608.
Ullah, S.N., Khuda, N.E.S., Fook Hou, L., Suntharavadivel, T., Albermani, F., 2020. Deep undrained bearing capacity of rectangular foundations in uniform strength clay. J. Geotech. Geoenviron. Eng. 146 (10), 04020105.
Vardanega, P.J., Bolton, M.D., 2013. Stiffness of clays and silts: Normalizing shear modulus and shear strain. J. Geotech. Geoenviron. Eng. 139 (9), 1575–1589.
Viggiani, G., Atkinson, J., 1995. Stiffness of fine-grained soil at very small strains. Geotechnique 45 (2), 249–265.
Wang, D., White, D.J., Randolph, M.F., 2010. Large-deformation finite element analysis of pipe penetration and large-amplitude lateral displacement. Can. Geotech. J. 47 (8), 842–856.
Wang, D., Bienen, B., Nazem, M., Tian, Y., Zheng, J., Pucker, T., Randolph, M.F., 2015. Large deformation finite element analyses in geotechnical engineering. Comput. Geotech. 65, 104–114.
Wang, C., Carter, J., 2002. Deep penetration of strip and circular footings into layered clays. Int. J. Geomech. 2 (2), 205–232.
Wang, L., Liu, X., Wu, W., El Naggar, M.H., Mei, G., Wen, M., Xu, M., Liu, H., Lu, C., 2023. Nonlinear analysis of laterally loaded single pile in layered soil based on conical strain wedge model. Ocean Eng. 280, 114699.
Xiao, Z., Fu, D., Zhou, Z., Lu, Y., Yan, Y., 2019. Effects of strain softening on the penetration resistance of offshore bucket foundation in nonhomogeneous clay. Ocean Eng. 193, 106594.
Yang, Z., Zou, X., Chen, S., 2024. Interaction model for horizontal dynamic response of monopile-friction wheel composite foundation in marine area. Comput. Geotech. 166, 105999.
Yu, H.-S., 2000. Cavity Expansion Methods in Geomechanics. Springer Science and Business Media.
Yu, L., Liu, J., Kong, X., Hu, Y., 2008. Three-dimensional RITSS large displacement finite element method for penetration of foundations into soil. Comput. Geotech. 35 (3), 372–382.
Zhang, Y., Bienen, B., Cassidy, M.J., Gourvenec, S., 2012. Undrained bearing capacity of deeply buried flat circular footings under general loading. J. Geotech. Geoenviron. Eng. 138 (3), 385–397.
Zhang, W., Pan, Y., Bransby, F., 2022. Scale effects during cone penetration in spatially variable clays. Geotechnique 72 (1), 78–90.
Zhang, W., Randolph, M.F., 2020. A smoothed particle hydrodynamics modelling of soil–water mixing and resulting changes in average strength. Int. J. Numer. Anal. Meth. Geomech. 44 (11), 1548–1569.
Zhang, W., Wang, D., Randolph, M.F., Puzrin, A.M., 2015. Catastrophic failure in planar landslides with a fully softened weak zone. Géotechnique 65 (9), 755–769.
Zhou, H., 2008. Numerical study of geotechnical penetration problems for offshore applications. The University of Western Australia. Ph. D. Thesis.
Zhou, S., Zhou, M., Zhang, X., Tian, Y., 2021. Installation of caisson in non-uniform clay interbedded with a sand layer. Comput. Geotech. 140, 104439.